THE EUROPEAN
PHYSICAL JOURNAL C

Transversity and heavy quark production on hadron colliders

G. P. Zhang[a]

Department of physics, Yunnan University, Kunming 650091, Yunnan, China

Abstract The azimuthal asymmetry of heavy quarks production on double polarized proton–proton and proton–antiproton colliders are studied in this work at next-to-leading order in α_s, with some details included. The purpose is to see whether the effect of extracted transversity distribution functions can be seen on present and near future colliders. All analytic one-loop hard coefficients are given. Numerical results for the asymmetry on proton–(anti)proton colliders are presented.

1 Introduction

Transversity distribution function of quark is one of three twist-2 parton distribution functions (PDFs), which reflects the spin structure of proton [1–4]. Compared with other two PDFs, the extraction of transversity PDF is much more difficult. Due to its chiral-odd nature, it must convolute with another chiral-odd distribution or fragmentation function to form an observable. Through many years of efforts, now the transversity PDFs in valence region are available. There are two independent extraction formalisms in literature: One is based on transverse momentum dependent (TMD) factorization formalism, for which one has to determine Collins function at the same time [5–7]; Another one is based on collinear formalism, with Di-hadron fragmentation functions as input [8]. Within uncertainty range the results of these two formalisms are in agreement. In both schemes sea transversity cannot be determined at present. On the other hand, double spin asymmetry (DSA), including double polarized Drell–Yan, single jet or photon production (see e.g., [3,9–15]) has been proposed for a long time to extract transversity distributions. Since sea transversity is expected to be small, the resulting DSAs on proton–proton colliders, such as RHIC [16], are usually very small. However, as long as the production rate is high, it is not hopeless to see the effect of

[a] e-mail: zgp-phys@pku.edu.cn (corresponding author)

transversity PDFs. Besides lepton pair, jet and photon, the heavy quark(such as bottom) production rate on RHIC is also very high, which is of order $10^3 pb$, thus may provide some opportunities to see the effect of sea transversity or give a bound to sea transversity. If polarized anti-proton beam is available in future, as proposed by PAX collaboration at GSI [17,18], valence transversity PDFs will be detected directly through double polarized Drell–Yan process. As an important background to polarized Drell–Yan, heavy quark production has to be known. In this work, we study the production rate of single inclusive heavy quark in hadron-hadron collision with the initial two hadrons transversely polarized. The result may help to check extracted transversity PDFs.

The structure of this paper is as follows: In Sect. 2, we make clear our formalism; in Sect. 3, we present virtual and real one-loop corrections and the subtracted result. Some details for the reduction and calculation scheme of real correction will be given;in Sect. 4, the numerical results on proton–(anti)proton colliders are described and Sect. 5 is our summary.

2 Formalism and tree level result

The process we want to study is

$$h_A(P_A, s_{a\perp}) + h_B(P_B, s_{b\perp}) \rightarrow Q(p_1) + X, \qquad (1)$$

where h_A, h_B with momentum P_A, P_B are two transversely polarized hadrons, which can be proton or anti-proton in our case. $s_{a\perp}$, $s_{b\perp}$ are corresponding spin vectors, which are perpendicular to momenta $\vec{P}_A$, $\vec{P}_B$ in the center of mass system (cms) of initial hadrons. $Q(p_1)$ is the detected heavy quark (bottom or charm), with momentum p_1. Our calculation will be performed in cms of initial hadrons.

For heavy quark (charm or bottom) production, the quark mass is much greater than the typical hadron scale of QCD, i.e. Λ_{QCD}, thus perturbative calculation is allowed. Besides,
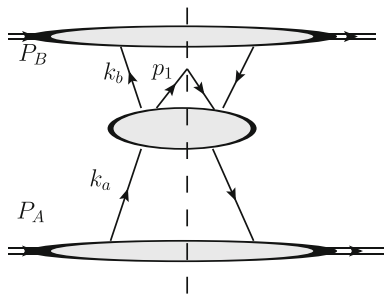
Fig. 1 Leading region for heavy quark production. The central bubble represents hard region, and upper and lower bubbles represent collinear regions

we require the detected heavy quark has a large transverse momentum $p_{1\perp}$, which is usually larger than quark mass. By combining these two hard scales together, the typical hard scale for this process could be taken as the transverse energy defined as $E_{1\perp} = \sqrt{\vec{p}_{1\perp}^2 + m^2}$. In the following, we will give the leading power cross sections under the expansion in $\Lambda_{QCD}/E_{1\perp}$, which is called twist-2 contribution.

The calculation of twist-2 cross section for heavy quark production is very standard. Unpolarized cross section at next-to-leading order (NLO) in strong coupling α_s expansion has been calculated long before [19–21]. So far, even next-to-next-to-leading order (NNLO) result is available(see [22] for example). Here we just give a simple derivation of the factorization formula. More formal discussions can be found in [23] and reference therein.

Throughout the paper, we work in cms of initial hadrons and use light-cone coordinates. For any four vector a^μ, its components are denoted by $a^\mu = (a^+, a^-, a^\mu_\perp)$, with $a^\pm = (a^0 \pm a^3)/\sqrt{2}$. In addition, $\vec{P}_A$ is along $+z$ axis. Under high energy limit $E_{1\perp} \gg \Lambda_{QCD}$, the hadron masses can be ignored and then $P^\mu_A \simeq (P^+_A, 0, 0)$, $P^\mu_B \simeq (0, P^-_B, 0)$. For convenience we introduce a transverse metric:

$$g^{\mu\nu}_\perp = g^{\mu\nu} - \frac{P^\mu_A P^\nu_B + P^\nu_A P^\mu_B}{P_A \cdot P_B}, \tag{2}$$

then the transverse components of any vector a^μ is given by $a^\mu_\perp = g^{\mu\nu}_\perp a_\nu$.

Under high energy limit, $E_{1\perp} \gg \Lambda_{QCD}$, collinear partons give leading power or twist-2 contribution. The leading region for quark contribution is shown in Fig. 1, where the momenta of partons k_a, k_b are collinear to external momenta P_A, P_B, respectively. That is,

$$k^\mu_a = (k^+_a, k^-_a, k^\mu_{a\perp})$$
$$\simeq E_{1\perp}(1, \lambda^2, \lambda),$$
$$k^\mu_b \simeq E_{1\perp}(\lambda^2, 1, \lambda), \lambda$$
$$\simeq \Lambda_{QCD}/E_{1\perp} \ll 1. \tag{3}$$

According to Fig. 1, the cross section is written as

$$d\sigma(s_{a\perp}, s_{b\perp}) = \frac{1}{2S} \int \frac{d^{n-1}p_1}{(2\pi)^{n-1}2E_1} \int d^n k_a d^n k_b$$
$$\times \int \frac{d^n\xi_a}{(2\pi)^n} \frac{d^n\xi_b}{(2\pi)^n} e^{ik_a \cdot \xi_a} e^{ik_b \cdot \xi_b} H^{mn}_{ij}(k_a, k_b, p_1)$$
$$\times \langle P_A s_a | \bar{\psi}_j(0) \psi_i(\xi_a) | P_A s_a \rangle$$
$$\times \langle P_B s_b | \psi_n(0) \bar{\psi}_m(\xi_b) | P_B s_b \rangle, \quad S = (P_A + P_B)^2, \tag{4}$$

where ij, mn are color and Dirac indices of partons, and H^{mn}_{ij} is the hard part in which inner propagators are far off-shell. Since $k_{a\perp}$, $k_{b\perp}$ are much smaller than $E_{1\perp}$ in H^{mn}_{ij}, they can be ignored at leading power level. This gives twist-2 hard coefficients. After this approximation, $k_{a\perp}$, k^-_a and $k_{b\perp}$, k^+_b can be integrated over in the correlation functions. Then,

$$d\sigma(s_{a\perp}, s_{b\perp}) = \frac{1}{2S} \int \frac{d^{n-1}p_1}{(2\pi)^{n-1}2E_1} \int dk^+_a dk^-_b H^{mn}_{ij}(k^+_a, k^-_b, p_1)$$
$$\times \int \frac{d\xi^-_a}{2\pi} e^{ik^+_a \xi^-_a} \langle P_A s_a | \bar{\psi}_j(0) \psi_i(\xi^-_a) | P_A s_a \rangle$$
$$\times \int \frac{d\xi^+_b}{2\pi} e^{ik^-_b \xi^+_b} \langle P_B s_b | \psi_n(0) \bar{\psi}_m(\xi^+_b) | P_B s_b \rangle. \tag{5}$$

The correlation functions defined on the light-cone can be projected to PDFs [2] as

$$\int \frac{d\xi^-}{2\pi} e^{-i\xi^- x P^+_A} \langle P_A s | \bar{\psi}_j(\xi^-) \psi_i(0) | P_A s \rangle$$
$$= \frac{1}{2N_c} \delta_{ij} \left[\gamma_5 \slashed{s}_\perp \gamma^- h_1(x) + \gamma^- f_1(x) \right]_{ij}, \tag{6}$$

which is for quark PDF and

$$\int \frac{d\xi^-}{2\pi} e^{-i\xi^- x P^+_A} \langle P_A s | \psi_i(\xi^-) \bar{\psi}_j(0) | P_A s \rangle$$
$$= \frac{1}{2N_c} \delta_{ij} \left[\gamma_5 \slashed{s}_\perp \gamma^- \bar{h}_1(x) + \gamma^- \bar{f}_1(x) \right]_{ij}, \tag{7}$$

which is for anti-quark PDF. Since we only consider transverse spin effect in this work, we have ignored the longitudinal components of spin vectors in the two equations above.

Apparently, chiral-odd PDF h_1 will not combine with chiral-even PDF f_1 to give a nonzero cross section since light quark is taken as massless. Our final factorization formula is

$$\frac{d\sigma(s_{a\perp}, s_{b\perp})}{dy d^2 p_{1\perp}}$$
$$= \frac{d\sigma_{unp}}{dy d^2 p_{1\perp}} + \frac{d\Delta\sigma}{dy d^2 p_{1\perp}}, \tag{8}$$

and

$$\frac{d\sigma_{unp}}{dyd^2p_{1\perp}}$$

$$= \int dx_a dx_b f_1(x_a, \mu) \bar{f}_1(x_b, \mu) \frac{d\hat{\sigma}_{unp}(k_a^+, k_b^-, p_1)}{dyd^2p_{1\perp}},$$

$$\frac{d\Delta\sigma}{dyd^2p_{1\perp}}$$

$$= \int dx_a dx_b h_1(x_a, \mu) \bar{h}_1(x_b, \mu) \frac{d\Delta\hat{\sigma}(k_a^+, k_b^-, p_1)}{dyd^2p_{1\perp}}, \quad (9)$$

where $d\hat{\sigma}_{unp}$ is spin independent partonic cross section and $d\Delta\hat{\sigma}$ is spin dependent part which is proportional to $s_{a\perp}$ and $s_{b\perp}$. The explicit formulas for these two partonic cross sections are

$$\frac{d\hat{\sigma}_{unp}}{dyd^2p_{1\perp}} = \frac{1}{8(2\pi)^3}\left(\frac{1}{2N_c}\right)^2 H_{ij}^{mn}(k_a^+, k_b^-, p_1)$$

$$\times [\delta_{ij}\gamma_{ij}^-][\delta_{mn}\gamma_{mn}^+],$$

$$\frac{d\Delta\hat{\sigma}}{dyd^2p_{1\perp}} = \frac{1}{8(2\pi)^3}\left(\frac{1}{2N_c}\right)^2 H_{ij}^{mn}(k_a^+, k_b^-, p_1)\delta_{ij}$$

$$\times [\gamma_5\not{s}_{a\perp}\gamma^-]_{ij}\delta_{mn}[\gamma_5\not{s}_{b\perp}\gamma^+]_{mn}. \quad (10)$$

Note that H_{ij}^{mn} is obtained by removing parton propagators connecting hard part and collinear(or jet) part in Fig. 1. δ_{ij}, δ_{mn} are color matrices in color space.

Next we analyze the spin structure of polarized partonic cross section $d\Delta\hat{\sigma}$. Since the two spin vectors are transverse and there is only one transverse momentum $p_{1\perp}$ in this process, we must have two structure functions $F_{1,2}$, which are defined as

$$\frac{d\Delta\hat{\sigma}}{dyd^2p_{1\perp}}$$

$$\equiv s_{a\perp}^\alpha s_{b\perp}^\beta W_\perp^{\alpha\beta}(k_a^+, k_b^-, p_1)$$

$$= s_{a\perp}^\alpha s_{b\perp}^\beta\left[F_1\left(g_\perp^{\alpha\beta} - \frac{(n-2)p_{1\perp}^\alpha p_{1\perp}^\beta}{p_{1\perp}^2}\right) + F_2 g_\perp^{\alpha\beta}\right],$$

$$p_{1\perp}^2 = -\vec{p}_{1\perp}^2 < 0. \quad (11)$$

There is no anti-symmetric tensor $\epsilon^{\mu\nu\rho\tau}$ in the tensor decomposition, because in the Dirac trace γ_5 appears in pair. Now $F_{1,2}$ do not contain spin vectors any more, they can be calculated in the same way as that for unpolarized partonic cross section. Since both ultra-violate (UV) and infra-red (IR) divergences will appear in $F_{1,2}$ beyond tree level, we make use of dimensional regularization for these two kinds of divergences. The space-time dimension is $n = 4 - \epsilon$. Unless declared explicitly, $1/\epsilon$ represents UV or IR poles. After renormalization and subtraction of IR divergences we take the limit $\epsilon \to 0$.

Now the spin dependence is clear, and the azimuthal angle dependence can be obtained. We consider a special case, in which $\vec{s}_{a\perp} \parallel \vec{s}_{b\perp}$. Other spin configurations can be considered, but one cannot get more information. Suppose both $\vec{s}_{a\perp}$ and $\vec{s}_{b\perp}$ are along $+x$-axis and the azimuthal angle of $\vec{p}_{1\perp}$ relative to $+x$-axis is ϕ. We have

$$\frac{d\Delta\hat{\sigma}}{dyd^2p_{1\perp}} = |\vec{s}_{a\perp}||\vec{s}_{b\perp}|\left[\left(1 - \frac{\epsilon}{2}\right)F_1(p_{1\perp}^2)\cos 2\phi\right.$$

$$\left. - \frac{\epsilon}{2}F_1(p_{1\perp}^2) - F_2(p_{1\perp}^2)\right]. \quad (12)$$

What we are interested in is the $\cos 2\phi$ distribution. Especially, in our calculation we find that at one-loop level ϵF_1 and F_2 can be ignored, because they are $O(\epsilon)$ after renormalization and collinear subtraction. In the following we will only consider the contribution of F_1. By substituting partonic cross section into Eq. (9), the hadron cross section is

$$\frac{d\sigma(s_{a\perp}, s_{b\perp})}{dyd^2p_{1\perp}} = \int dx_a dx_b\left[f_1(x_a, \mu)\bar{f}_1(x_b, \mu)\right.$$

$$\times \frac{d\hat{\sigma}_{unp}(k_a^+, k_b^-, p_1)}{dyd^2p_{1\perp}} + \cos 2\phi|\vec{s}_{a\perp}||\vec{s}_{b\perp}|$$

$$\left. h_1(x_a, \mu)\bar{h}_1(x_b, \mu)F_1(k_a^+, k_b^-, p_1)\right]. \quad (13)$$

Now the double spin asymmetry (DSA) is defined as

$$A_{TT} = \frac{\int_0^{2\pi} d\phi \cos 2\phi \left[d\sigma(s_{a\perp}, s_{b\perp}) - d\sigma(s_{a\perp}, -s_{b\perp})\right]}{\int_0^{2\pi} d\phi \left[d\sigma(s_{a\perp}, s_{b\perp}) + d\sigma(s_{a\perp}, -s_{b\perp})\right]}, \quad (14)$$

where the azimuthal angle of detected heavy quark, ϕ, is integrated over. Expressed in partonic quantities, A_{TT} is

$$A_{TT} = |\vec{s}_{a\perp}||\vec{s}_{b\perp}|\frac{\pi}{2}\frac{\int dx_a dx_b h_1(x_a, \mu)\bar{h}_1(x_b, \mu)F_1}{\int dx_a dx_b f_1(x_a, \mu)\bar{f}_1(x_b, \mu)\frac{d\hat{\sigma}_{unp}}{dyd\vec{p}_1^2}}. \quad (15)$$

Note that we have used the relation $\pi d\sigma_{unp}/dyd^2p_{1\perp} = d\sigma_{unp}/dyd\vec{p}_{1\perp}^2$ for unpolarized cross section.

For the calculation of partonic cross sections, we use the Lorentz invariants defined in [19], that is,
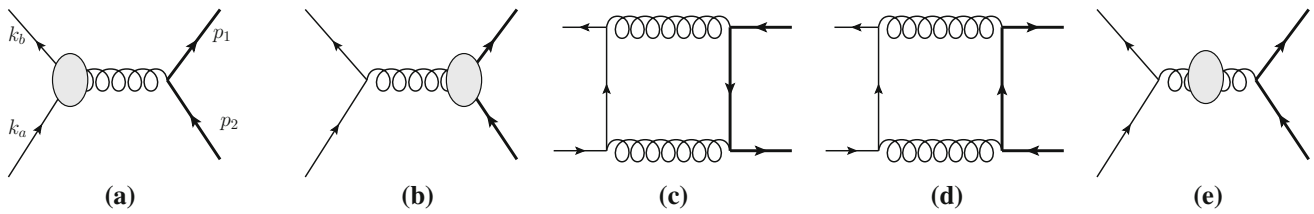
Fig. 2 Virtual corrections to the amplitude, where the bubbles in **a**, **b** represent vertex insertion and the bubble in **e** represents the insertion of gluon self-energy in Feynman gauge. Self-energy insertion to external legs is not shown but included in the calculation. Thick lines represent heavy quarks

$$\tau_1 = \frac{k_a \cdot p_1}{k_a \cdot k_b}, \quad \tau_2 = \frac{k_b \cdot p_1}{k_a \cdot k_b},$$

$$\rho = \frac{4m^2}{s}, \quad \tau_x \equiv 1 - \tau_1 - \tau_2, \quad s = (k_a + k_b)^2. \quad (16)$$

Generally, partonic structure function F_1 can be organized in a neat way as done in [19], i.e.,

$$F_1 = \Delta H_d \delta(\tau_x) + \Delta H_p \left(\frac{1}{\tau_x}\right)_+ + \Delta H_l \left(\frac{\ln \tau_x}{\tau_x}\right)_+,$$

$$\Delta H_d = \frac{\alpha_s^2}{s^2} \left[\Delta h_d^{(0)} + \frac{\alpha_s}{2\pi} \Delta h_d^{(1)} + \cdots\right],$$

$$\Delta H_p = \frac{\alpha_s^2}{s^2} \left[\frac{\alpha_s}{2\pi} \Delta h_p^{(1)} + \cdots\right],$$

$$\Delta H_l = \frac{\alpha_s^2}{s^2} \left[\frac{\alpha_s}{2\pi} \Delta h_l^{(1)} + \cdots\right]. \quad (17)$$

The plus function is the standard one [19]. Tree level result is given by the process $q(k_a)\bar{q}(k_b) \rightarrow Q(p_1) + \bar{Q}$, and we get

$$\Delta h_d^{(0)} = -\frac{C_F}{2N_c}(\rho - 4\tau_1(1 - \tau_1)) \left[1 + \frac{\epsilon}{2} + \frac{\epsilon^2}{4} + O(\epsilon^3)\right]. \quad (18)$$

For F_2 we get

$$F_2 = \frac{\alpha_s^2}{s^2} \frac{C_F}{2N_c} \frac{\epsilon}{2} [\rho + 2 - 4\tau_1(1 - \tau_1)]\delta(\tau_x). \quad (19)$$

As we see, F_2 is $O(\epsilon)$. To one-loop level, F_2 can have a finite part, but it has been checked explicitly that the finite part is removed by renormalization and collinear subtraction. The resulting F_2 is still $O(\epsilon)$ and can be ignored. In the following we will not discuss F_2 any more.

For unpolarized partonic cross section, similar hard coefficients are defined as follows

$$\frac{d\hat{\sigma}^{unp}}{dy d^2 p_{1\perp}} = H_d \delta(\tau_x) + H_p \left(\frac{1}{\tau_x}\right)_+ + H_l \left(\frac{\ln \tau_x}{\tau_x}\right)_+. \quad (20)$$

Compared with the decomposition of F_1, all $\Delta H_{d,p,l}$ are replaced by $H_{d,p,l}$. The expansion of $H_{d,p,l}$ in terms of $h_{d,p,l}$ is the same as that for $\Delta H_{d,p,l}$. Tree level unpolarized result from $q\bar{q}$ scattering is

$$h_d^{(0)}\Big|_{q\bar{q}} = \frac{C_F}{2N_c} \left[2 + \rho - 4\tau_1(1 - \tau_1) - \epsilon + O(\epsilon^3)\right]. \quad (21)$$

3 One-loop correction

3.1 One-loop virtual correction

All diagrams appearing in virtual correction are shown in Fig. 2. Self-energy insertions to external lines are trivial and not shown, but included in our calculation.
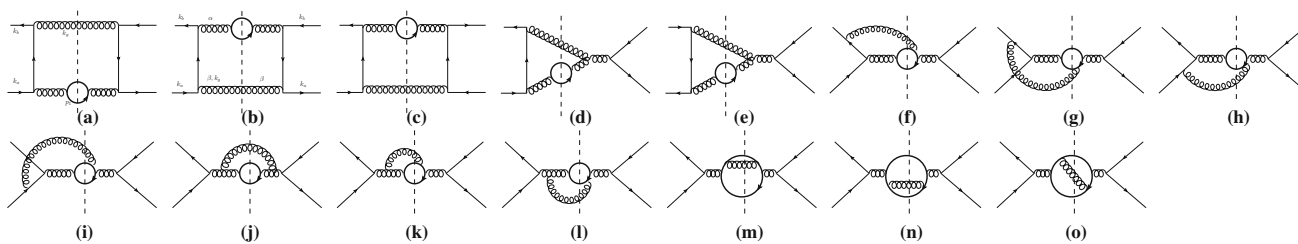
Calculating these diagrams is very straightforward. The tensor integrals are reduced by FIRE [24]. Resulting scalar integrals are standard and can be found for example in [20,25]. We note that by integration by part relations (IBPs) for integral reduction, the divergent pole $1/\epsilon$ may transfer from tensor or scalar integrals to reduced coefficients. In order to get finite result, the resulting scalar integrals should be expanded to higher orders in ϵ. In our case, we find it necessary to expand bubble and tadpole integrals to $O(\epsilon)$. The bubble and tadpole integrals are listed in Appendix A.

There are UV, soft and collinear divergences in virtual correction. But a simple analysis indicates these divergences are independent of the polarization status of initial partons. This is confirmed by our explicit calculation. The divergent hard coefficients from Fig. 2 are

$$\{h_d^{(1)}, \Delta h_d^{(1)}\} = \{h_d^{(0)}, \Delta h_d^{(0)}\} 16\pi R_\epsilon \left(\frac{\mu^2}{m^2}\right)^{\epsilon/2}$$

$$\times [C_F \Delta G_1 + C_A \Delta G_2 + \Delta G_3],$$

$$R_\epsilon \equiv \frac{(4\pi)^{\epsilon/2}}{8\pi \Gamma(1 - \epsilon/2)},$$

Fig. 3 Diagrams for real corrections. Conjugated diagrams are not shown, but included in the calculation

$$\Delta G_1 = -\frac{4}{\epsilon^2} - \frac{2}{\epsilon}$$

$$\times \left[\frac{2-\rho}{2\sqrt{1-\rho}} \ln \frac{1-\sqrt{1-\rho}}{1+\sqrt{1-\rho}} + 1 \right.$$

$$\left. + \ln \frac{\rho}{4} + 4 \ln \frac{1-\tau_1}{\tau_1} \right],$$

$$\Delta G_2 = \frac{1}{\epsilon} \left[\frac{2-\rho}{2\sqrt{1-\rho}} \ln \frac{1-\sqrt{1-\rho}}{1+\sqrt{1+\rho}} \right.$$

$$\left. + \frac{11}{3} - \ln \frac{\rho}{4} + 2 \ln \frac{(1-\tau_1)^2}{\tau_1} \right],$$

$$\Delta G_3 = -\frac{2(2+n_F)}{3\epsilon}, \tag{22}$$

where n_F is the number of light fermion flavors. Throughout this paper, it is equal to 3. Both charm and bottom are included in the fermion loops appearing in gluon self-energy, i.e., Fig. 2e. Wave function renormalization and UV counter terms(c.t.) give

$$\{h_d^{(1)}, \Delta h_d^{(1)}\}\Big|_{\text{wave+c.t.}}$$

$$= \{h_d^{(0)}, \Delta h_d^{(0)}\} \left[\frac{2\pi}{\alpha_s} \left(2(Z_2 - 1) + 2(Z_2^{(m)} - 1) \right) \right.$$

$$\left. - 16\pi R_\epsilon \frac{11C_A + 6C_F - 2(2+n_F)}{3\epsilon} \right], \tag{23}$$

The factor $2\pi/\alpha_s$ is caused by the definition of $h_d^{(1)}$ or $\Delta h_d^{(1)}$. Wave function renormalization constants for massless and massive fermions are

$$Z_2 - 1 = \frac{g_s^2 C_F}{16\pi^2} \left(\frac{2}{\epsilon_{IR}} - \gamma_E + \ln 4\pi \right),$$

$$Z_2^m - 1 = -\frac{g_s^2 C_F}{16\pi^2} \left[2 \left(\frac{2}{\epsilon_{IR}} - \gamma_E + \ln 4\pi \right) \right.$$

$$\left. + 3 \ln \frac{\mu^2}{m^2} + 4 \right]. \tag{24}$$

For convenience, we have removed UV poles by using $\overline{\text{MS}}$ renormalization scheme. In addition, mass renormalization for massive quark is done in pole mass scheme. The renormalized mass m is a physical mass and does not depend on renormalization scale. For simplicity, we do not plan to show the finite corrections in this paper, but leave them in the mathematica files, which can be obtained from author if required.

3.2 One-loop real correction

Real correction is given by following process,

$$q(k_a) + \bar{q}(k_b) \rightarrow Q(p_1) + \bar{Q}(p_2) + g(k_g). \tag{25}$$

To get the cross section we calculate the cut diagrams in Fig. 3. The partonic cross sections are obtained according to Eq. (10). Now the hard part H_{ij}^{mn} in Eq. (10) contains a two-body phase space integration for p_2 and k_g. By moving heavy quark with momentum p_1 from final state to initial state, the sum of these cut diagrams is equal to the cut amplitude of following forward scattering

$$q(k_a) + \bar{q}(k_b) + \bar{Q}(-p_1) \rightarrow q(k_a) + \bar{q}(k_b) + \bar{Q}(-p_1), \tag{26}$$

with intermediate on-shell state being $|\bar{Q}(p_2), g(k_g)\rangle$.

Then, the involved cut tensor integrals can be reduced to scalar ones in the same way as uncut tensor integrals [26]. FIRE [24] with IBPs incorporated is a particularly suitable tool for this purpose. After reduction, there are only six types of master integrals, which are shown in Fig. 4.

The general form of the master integral is

$$I_r = \int \frac{d^n k_g}{(2\pi)^n} \frac{(2\pi)^2 \delta_1 \delta_2}{N_1^{i_1} N_2^{i_2}}, \qquad \delta_1 \equiv \delta(k_g^2),$$

$$\delta_2 \equiv \delta((k_a + k_b - p_1 - k_g)^2 - m^2), \tag{27}$$

where N_1, N_2 are denominators of uncut propagators. These I_r integrals are in the standard form, i.e., $i_{1,2} = 0$ or 1.

To calculate I_r it is convenient to work in the frame with $\vec{q} = 0$, where $q = k_a + k_b - p_1$. First, the energy of gluon k_g^0 can be integrated out by using the two delta functions. Then,
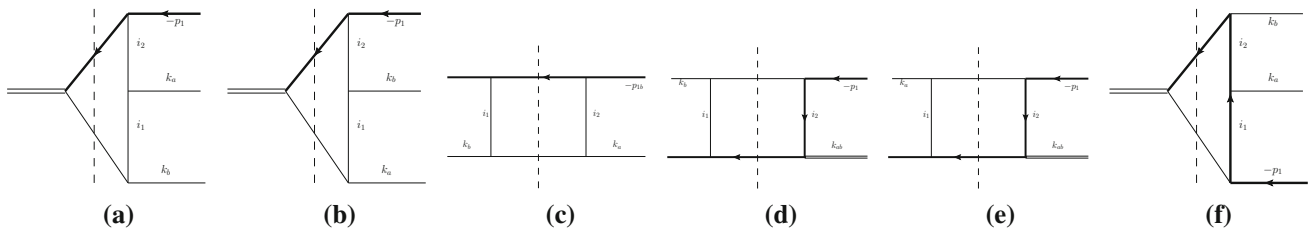
Fig. 4 Master integrals for real correction. $i_{1,2} = 0, 1$ are the indices of propagators. $k_{ab} = k_a + k_b$, $p_{1a} = p_1 - k_a$, $p_{1b} = p_1 - k_b$. External momenta on left-hand side of the cut are ingoing and those on right-hand side of the cut are outgoing. The thick line is for heavy quark. The thin real line is for massless parton. Off-shell external momenta are represented by double line

$$I_r = \left(\frac{\mu}{k_g^0}\right)^\epsilon \frac{k_g^0}{4q^0} \int d\Omega_{n-1} \frac{1}{N_1^{i_1} N_2^{i_2}}, \qquad (28)$$

with k_g^0 the energy of final gluon. Explicitly, $k_g^0 = s\tau_x/(2q^0)$ and $q^0 = \sqrt{m^2 + s\tau_x}$. $d\Omega_{n-1}$ is the angular integration measure for $\vec{k}_g$, which is defined in $n - 1 = 3 - \epsilon$ dimensional space. I_r may contain collinear and soft divergences. Different from virtual correction, these two divergences in real correction can be separated very easily. Soft divergence corresponds to the singularity at $\tau_x = 0$. If I_r is singular under soft limit $\tau_x \to 0$, N_1 or N_2 must be proportional to k_g^0. Then, k_g^0 can be extracted from N_1 or N_2. This implies we can define an integral $\tilde{I}_r$ as follows, which is regular under soft limit.

$$I_r = \left(\frac{\mu}{k_g^0}\right)^\epsilon \tau_x^k s^{-i_1-i_2} \tilde{I}_r. \qquad (29)$$

τ_x^k is extracted from N_1, N_2. If I_r contains soft divergence, $k = -1$. In this way, collinear divergence is included in $\tilde{I}_r$ and soft divergence is given by the expansion of $\tau_x^{-1-\epsilon}$ in ϵ, i.e.,

$$\tau_x^{-1-\epsilon} = \frac{1}{-\epsilon}\delta(\tau_x) + \left(\frac{1}{\tau_x}\right)_+ - \epsilon\left(\frac{\ln\tau_x}{\tau_x}\right)_+. \qquad (30)$$

The plus function is the standard one [19].

The angular integrals $\tilde{I}_r$ can be classified into following six types.

$$R_1(w) = \int d\Omega_{n-1} \frac{1}{1 + \vec{a}\cdot\vec{k}} \frac{1}{1 + \vec{b}\cdot\vec{k}},$$

$$R_2(\Delta, w) = \int d\Omega_{n-1} \frac{1}{1 + \vec{a}\cdot\vec{k}} \frac{1}{\Delta + \vec{b}\cdot\vec{k}},$$

$$R_3(\delta, \Delta, w) = \int d\Omega_{n-1} \frac{1}{\delta + \vec{a}\cdot\vec{k}} \frac{1}{\Delta + \vec{b}\cdot\vec{k}},$$

$$R_4 = \int d\Omega_{n-1} \frac{1}{1 + \vec{a}\cdot\vec{k}},$$

$$R_5(\delta) = \int d\Omega_{n-1} \frac{1}{\delta + \vec{a}\cdot\vec{k}},$$

$$R_6 = \int d\Omega_{n-1}. \qquad (31)$$

$\vec{k}, \vec{a}, \vec{b}$ are normalized to one, i.e., $|\vec{a}| = |\vec{b}| = |\vec{k}| = 1$. $w = 1/|\vec{a} - \vec{b}|$ and $\Delta > 1$, $\delta > 1$. $d\Omega_{n-1}$ is for $\vec{k}$.

Same as the reduction of virtual integrals, IR pole $1/\epsilon_{IR}$ may transfer from tensor integrals to reduced coefficients after FIRE reduction. Thus, some R_i should be expanded to higher orders of ϵ. In our case, we have checked that R_6 should be calculated to $O(\epsilon^2)$, while others, except for R_3, should be expanded to $O(\epsilon)$. We just need $O(\epsilon^0)$ part of R_3. By making use of Feynman parameters, these R_i are calculated and the results are given in Appendix B. These results are compared with known results in [20]. Numerically, they are the same.

In real correction, ΔH_d and H_d represent soft gluon contribution, because $\tau_x = 0$. These soft contributions can be obtained by eikonal approximation and are factorized diagram by diagram. Thus, we expect the real corrections to ΔH_d and H_d are the same. The explicit calculation confirms this. Interestingly, such soft correction for unpolarized $q\bar{q}$ scattering has been given in [21]. For convenience, we show the result of [21] here.

$$\left\{\Delta h_d^{(1)}, h_d^{(1)}\right\} = \left\{\Delta h_d^{(0)}, h_d^{(0)}\right\} \frac{1}{2} e^{-\frac{\epsilon}{2}(\gamma_E - \ln 4\pi)} \left(\frac{s^2}{\mu^2 m^2}\right)^{-\epsilon/2}$$

$$\times \left[C_F K_{soft}^F + C_A K_{soft}^A\right],$$

$$K_{soft}^F = \frac{16}{\epsilon^2} - \frac{8}{\epsilon}\ln y + 2\ln^2 y + 4Li_2(1 - y)$$

$$+ 4\left(1 - \frac{2m^2}{s}\right)\frac{1}{\beta}\left\{\frac{2}{\epsilon}\ln x - \ln x + 2Li_2(x)\right.$$

$$+ 2Li_2(-x) - \ln^2 x + 2\ln x \ln(1 - x^2) - \zeta(2)\Big\}$$

$$+ \frac{8}{\epsilon} + 4 - \frac{32}{\epsilon}\ln\frac{t_1}{u_1}$$

$$- 16\ln x \ln\frac{t_1}{u_1} - 16Li_2\left(1 - \frac{u_1}{xt_1}\right)$$

$$+ 16Li_2\left(1 - \frac{t_1}{xu_1}\right) - 6\zeta(2),$$

$$K_{soft}^A = \frac{4}{\epsilon}\ln y - \ln^2 y - 2Li_2(1 - y)$$

$$- 2\left(1 - \frac{2m^2}{s}\right)\frac{1}{\beta}$$

$$\times \left\{\frac{2}{\epsilon}\ln x + 2Li_2(x) + 2Li_2(-x) - \ln^2 x\right.$$

$$+ 2\ln x \ln(1 - x^2) - \zeta(2)\Big\}$$

$$- \frac{12}{\epsilon}\ln\frac{u_1}{t_1} + 6\ln x \ln\frac{t_1}{u_1} - \ln^2 x + \ln^2\frac{t_1}{u_1}$$

$$- 6Li_2\left(1 - \frac{t_1}{xu_1}\right) + 6Li_2(1 - \frac{u_1}{xt_1}), \tag{32}$$

with

$$y = \frac{sm^2}{t_1 u_1}, \quad x = \frac{1-\beta}{1+\beta}, \quad \beta = \sqrt{1 - \frac{4m^2}{s}},$$

$$t_1 = (k_a - p_1)^2 - m^2 = -s\tau_1,$$

$$u_1 = (k_b - p_1)^2 - m^2 = -s\tau_2. \tag{33}$$

We have checked that this result, including the finite part, is the same as our result. This is a strong check for our reduction scheme and the calculation of real integrals.

In hard coefficients h_p and h_l, τ_x can be nonzero. Thus, h_p and Δh_p contain collinear divergence only. h_l, Δh_l are finite and given by $-\epsilon h_p$, $-\epsilon \Delta h_p$, respectively. The collinear divergence for transversely polarized $q\bar{q}$ scattering is

$$\Delta h_p^{(1)} = \Delta h_d^{(0)}\frac{-32\pi C_F R_\epsilon}{\epsilon \tau_1 \tau_2(\rho - 4\tau_1(1 - \tau_1))}\left(\frac{\mu^2}{m^2}\right)^{\epsilon/2}$$

$$\times (\rho - 4\tau_1\tau_2)(2\tau_1\tau_2 + \tau_x(1 - \tau_x)). \tag{34}$$

Note that because $\Delta h_d^{(0)} \propto (\rho - 4\tau_1(1 - \tau_1))$, $\Delta h_p^{(1)}$ is symmetric in τ_1, τ_2.

But the divergence of unpolarized $h_p^{(1)}$ is much more complicated,

$$h_p^{(1)} = h_d^{(0)}\frac{-16\pi C_F R_\epsilon}{\epsilon[2 + \rho - 4\tau_1(1 - \tau_1)]}\left(\frac{\mu^2}{m^2}\right)^{\epsilon/2}$$

$$\times \left[\rho\frac{-2(\tau_1^3 + \tau_2^3) + (\tau_1^2 + \tau_2^2)(1 + \tau_1^2 + \tau_2^2)}{\tau_1^2\tau_2^2}\right.$$

$$\left.+ \frac{r^6 - r^4(1 - \tau_x^2) - r^2(1 + 2\tau_x^2 + 8\tau_x^3 + \tau_x^4) + (1 - \tau_x^2)(1 + \tau_2^2)^2}{4\tau_1\tau_2(1 - \tau_1)(1 - \tau_2)}\right], \tag{35}$$

with $r = \tau_1 - \tau_2$. To understand the difference between $h_p^{(1)}$ and $\Delta h_p^{(1)}$ is interesting. First, Δh_p and h_p contain only collinear divergence. Except for the ladder diagrams Fig. 3a, b, all other diagrams generate collinear divergence just from longitudinal real gluon. For longitudinal gluon, Ward Identities can be applied and the summed result can be expressed as the convolution of tree level partonic cross section and gauge link correction to PDFs(see [27] for example). The latter is the same for unpolarized PDF and transversity PDF. However, the divergence from ladder diagram is different. Consider ladder diagram Fig. 3b. For unpolarized case, according to the formula Eq. (10), the contribution of this diagram is proportional to

$$I = \int d^n k_g \gamma^+ \gamma^\alpha \frac{\not{k}_a - \not{k}_g}{(k_a - k_g)^2}\gamma^\beta \gamma^- \gamma_\beta \frac{\not{k}_a - \not{k}_g}{(k_a - k_g)^2}\delta(k_g^2), \tag{36}$$

where γ^+, γ^- are the projection matrices for unpolarized PDF. Due to γ^-, the real gluon must be transverse, that is, $\gamma^\beta = \gamma_\perp^\beta$. Then, in collinear region, it is $k_{g\perp}$ in the numerator that gives leading power contribution. Because $\gamma_\perp^\beta \gamma^- = -\gamma^- \gamma_\perp^\beta$, the integral becomes

$$I = \int d^n k_g \left[\gamma^+ \gamma^\alpha \gamma^-\right]\frac{(2 - \epsilon)k_{g\perp}^2}{[(k_a - k_g)^2]^2}\delta(k_g^2). \tag{37}$$

It is clear that the part in brackets gives tree level result and I contains a collinear divergence. On the other hand, for transversity contribution, this diagram is proportional to

$$\Delta I = \int d^n k_g (\gamma_5 \not{s}_{b\perp}\gamma^+)\gamma^\alpha$$

$$\times \frac{\not{k}_a - \not{k}_g}{(k_a - k_g)^2}\gamma^\beta (\gamma_5 \not{s}_{a\perp}\gamma^-)\gamma_\beta \frac{\not{k}_a - \not{k}_g}{(k_a - k_g)^2}\delta(k_g^2). \tag{38}$$

Due to the same reason, in collinear region ΔI receives contribution only from transverse gluon and can be written as

$$\Delta I = \int d^n k_g (\gamma_5 \not{s}_{b\perp} \gamma^+) \gamma^\alpha (-\gamma_5 \gamma^-)$$

$$\times \frac{\not{k}_{g\perp}}{(k_a - k_g)^2} \gamma_\perp^\beta (\not{s}_{a\perp}) \gamma_{\perp\beta} \frac{\not{k}_{g\perp}}{(k_a - k_g)^2} \delta(k_g^2). \qquad (39)$$

By power counting in collinear region, $k_{g\perp}$ in the other part of this diagram can be ignored, so, in the integrand the replacement $k_{g\perp}^\mu k_{g\perp}^\nu \to k_{g\perp}^2 g_\perp^{\mu\nu}/(2 - \epsilon)$ is allowed and we get

$$\Delta I = \int d^n k_g (\gamma_5 \not{s}_{b\perp} \gamma^+) \gamma^\alpha (-\gamma_5 \gamma^-)$$

$$\times \left[\gamma_\perp^\rho \gamma_\perp^\beta \not{s}_{a\perp} \gamma_{\perp\beta} \gamma_{\perp\rho} \right] \frac{k_{g\perp}^2/(2-\epsilon)}{[(k_a - k_g)^2]^2} \delta(k_g^2). \qquad (40)$$

Note that $\gamma_\perp^\beta \gamma_\perp^\mu \gamma_{\perp\beta} = \epsilon \gamma_\perp^\mu$. The quantity in brackets becomes

$$[\gamma_\perp^\rho \gamma_\perp^\beta \not{s}_{a\perp} \gamma_{\perp\beta} \gamma_{\perp\rho}] = \epsilon^2 \not{s}_{a\perp}. \qquad (41)$$

It is proportional to ϵ^2! Thus the integral ΔI and then the ladder diagram Fig. 3b just vanishes in collinear region when the limit $\epsilon \to 0$ is taken. This explains why $\Delta h_p^{(1)}$ is much simpler than $h_p^{(1)}$.

3.3 Subtraction and final result

To get the true one-loop contribution, we have to subtract collinear contributions from each diagram [27]. The subtraction is realized by following replacement in tree level hadron cross sections,

$$\{f_1(x_a, \mu^2), h_1(x_a, \mu^2)\}$$

$$\to \frac{\alpha_s}{2\pi} \frac{(4\pi)^{\epsilon/2}}{\Gamma(1 - \epsilon/2)} \left[\frac{2}{\epsilon_{UV}} - \frac{2}{\epsilon_{IR}} \right]$$

$$\times \int_{x_a}^1 \frac{d\xi_a}{\xi_a} \left\{ P_{qq}\left(\frac{x_a}{\xi_a}\right) f_1(\xi_a, \mu^2), P_{qq}^T\left(\frac{x_a}{\xi_a}\right) h_1(\xi_a, \mu^2) \right\}. \qquad (42)$$

The DGLAP evolution kernels (see [28–30] and reference therein) are

$$P_{qq}(x) = C_F \left[\frac{3}{2} \delta(1 - x) + \frac{1 + x^2}{(1 - x)_+} \right],$$

$$P_{qq}^T(x) = C_F \left[\frac{3}{2} \delta(1 - x) + \frac{2x}{(1 - x)_+} \right]. \qquad (43)$$

The UV pole $2/\epsilon_{UV}$ is removed by renormalization(in $\overline{\text{MS}}$-scheme) of bare transversity distribution which appearing in

tree level cross section. Then only IR pole should be preserved. The final subtraction terms are

$$\frac{d\sigma^{unp}}{dy d^2 p_{1\perp}}\bigg|_{sub} = \frac{\alpha_s C_F}{2\pi} \frac{(4\pi)^{\epsilon/2}}{\Gamma(1 - \frac{\epsilon}{2})} \left(\frac{-2}{\epsilon_{IR}}\right) \int dx_a dx_b f_1(x_a, \mu^2) \bar{f}_1(x_b, \mu^2)$$

$$\times \left[\frac{z_a P_{qq}(z_a)}{1 - \tau_1} H_d(z_a x_a, x_b) + \frac{z_b P_{qq}(z_b)}{1 - \tau_2} H_d(x_a, z_b x_b) \right]$$

$$= \frac{\alpha_s C_F}{2\pi} \frac{(4\pi)^{\epsilon/2}}{\Gamma(1 - \frac{\epsilon}{2})} \left(\frac{-2}{\epsilon_{IR}}\right)$$

$$\times \int dx_a dx_b f_1(x_a, \mu^2) \bar{f}_1(x_b, \mu^2)$$

$$\times \left[(3 - 2 \ln \tau_1(1 - \tau_1)) \delta(\tau_x) H_d(x_a, x_b) \right.$$

$$+ \frac{2}{(\tau_x)_+} \left(z_a(1 + z_a^2) H_d(z_a x_a, x_b) \right.$$

$$\left. + z_b(1 + z_b^2) H_d(x_a, z_b x_b) \right) \bigg],$$

$$\frac{d\Delta\sigma}{dy d^2 p_{1\perp}}\bigg|_{sub} = \cos(2\phi)|s_{a\perp}||s_{b\perp}| \frac{\alpha_s C_F}{2\pi} \frac{(4\pi)^{\epsilon/2}}{\Gamma(1 - \frac{\epsilon}{2})} \left(\frac{-2}{\epsilon_{IR}}\right)$$

$$\times \int dx_a dx_b h_1(x_a, \mu^2) \bar{h}_1(x_b, \mu^2)$$

$$\times \left[\frac{z_a P_{qq}^T(z_a)}{1 - \tau_1} \Delta H_d(z_a x_a, x_b) \right.$$

$$+ \left. \frac{z_b P_{qq}^T(z_b)}{1 - \tau_2} \Delta H_d(x_a, z_b x_b) \right]$$

$$= \cos(2\phi)|s_{a\perp}||s_{b\perp}| \frac{\alpha_s C_F}{2\pi} \frac{(4\pi)^{\epsilon/2}}{\Gamma(1 - \frac{\epsilon}{2})} \left(\frac{-2}{\epsilon_{IR}}\right)$$

$$\times \int dx_a dx_b h_1(x_a, \mu^2) \bar{h}_1(x_b, \mu^2)$$

$$\times \left[(3 - 2 \ln \tau_1(1 - \tau_1)) \delta(\tau_x) \Delta H_d(x_a, x_b) \right.$$

$$+ \frac{2}{(\tau_x)_+} \left(z_a^2 \Delta H_d(z_a x_a, x_b) + z_b^2 \Delta H_d(x_a, z_b x_b) \right) \bigg],$$

$$\qquad (44)$$

with $z_a = \tau_2/(1 - \tau_1)$, $z_b = \tau_1/(1 - \tau_2)$. The logarithm before $\delta(\tau_x)$ comes from the variable transformation in plus function [19],

$$\left(\frac{1}{a \tau_x}\right)_+ = \frac{1}{a} \left(\frac{1}{\tau_x}\right)_+ + \frac{\ln a}{a} \delta(\tau_x). \qquad (45)$$

Note that the subtraction terms contain no explicit $\ln \mu$. The final one-loop (order α_s^3) cross sections are given by

$$\frac{d\sigma}{dy d^2 p_{1\perp}} = \frac{d\sigma}{dy d^2 p_{1\perp}}\Big|_{real+vir} - \frac{d\sigma}{dy d^2 p_{1\perp}}\Big|_{sub}. \qquad (46)$$

The subtraction term is given by Eq. (44), and the divergent part of real and virtual corrections are given by Eqs. (22, 32, 34, 35). From these results, the soft divergences appearing in real and virtual corrections are cancelled, and the remaining collinear divergences are removed by the subtraction terms. The final one-loop cross section is then finite. Further, we note that massless wave function renormalization, UV counter terms and subtraction terms all are $\ln \mu$ independent. The $\ln \mu$ dependence comes from the loop integrals in Figs. 2, 3, and from the massive fermion wave function renormalization constant $Z_2^{(m)}$ in Eq. (24). The $\ln \mu$ dependence extracted from above results is

$$\frac{d\Delta\sigma}{dy d^2 p_{1\perp}}$$

$$= \int dx_a dx_b h_1(x_a, \mu^2) \bar{h}_1(x_b, \mu^2) \frac{\alpha_s^2}{s} \Delta h_d^{(0)}(x_a, x_b) \delta(\tau_x)$$

$$+ \int dx_a dx_b h_1(x_a, \mu^2) \bar{h}_1(x_b, \mu^2) \ln \frac{\mu^2}{m^2}$$

$$\times \left\{ \alpha_s \times (2b_0) \Delta H_d^{tree}(x_a, x_b) \delta(\tau_x) \right.$$

$$- \frac{\alpha_s C_F}{2\pi} \left[\frac{z_a}{1-\tau_1} P_{qq}^T(z_a) \Delta H_d^{tree}(z_a x_a, x_b) \right.$$

$$\left. \left. + \frac{z_b}{1-\tau_2} P_{qq}^T(z_b) \Delta H_d^{tree}(x_a, z_b x_b) \right] \right\} + \cdots, \qquad (47)$$

where $\cdots$ are of order α_s^3 and do not depend on $\ln \mu$ explicitly. Note that $\Delta H_d^{tree} = (\alpha_s^2/s) \Delta h_d^{(0)}$ and the μ dependence of α_s is given by RGE

$$\frac{\partial \alpha_s(\mu^2)}{\partial \ln \mu^2} = -b_0 \alpha_s^2(\mu^2), \ b_0 = \frac{11C_A - 2(2 + n_F)}{12\pi}. \qquad (48)$$

Now it is obvious that Eq. (47) is $\ln \mu$ independent up to $O(\alpha_s^4)$. For unpolarized cross section, the same conclusion holds by transparent replacement of PDFs and DGLAP evolution kernels. Now, we finish our calculation of one-loop correction to heavy quark production process. All results, including finite hard coefficients, are stored in mathematica files which can be obtained from author if required.

Before ending this section, we want to discuss the regularization of γ_5 in dimensional scheme. This problem, however, is related to the regularization of spin vector s^μ. For a consistent regularization scheme, if the momentum of a particle

is defined in n dimensional space, the related spin vector or polarization vector should also be defined in n dimensional space. For our case here, the hadron momenta P_A, P_B are external momenta, which are allowed to be constrained in 4 dimensional space. Thus, spin vectors s_a^μ, s_b^μ are defined in 4 dimensional space. Then, we consider HVBM scheme for γ_5 [31,32]. In this scheme γ_5 is defined in 4 dimensional space, i.e., $\gamma_5 = -i\gamma^0 \gamma^1 \gamma^2 \gamma^3$. Then, following identity holds

$$\gamma_5 \gamma^- \slashed{s}_{a\perp} = i\gamma^- \tilde{s}_{a\perp} \cdot \gamma, \ \tilde{s}_{a\perp}^\mu = \epsilon^{-+\mu\rho} s_{a\perp\rho}. \qquad (49)$$

This means γ_5 in spin projection operators can be eliminated. Then, partonic cross section can be written as

$$d\Delta\hat{\sigma} = \tilde{s}_{a\perp}^i \tilde{s}_{b\perp}^j W_{ij}(k_a, k_b, p_1), \qquad (50)$$

where i, j denote Lorentz indices in 4 dimensional space and μ, ν denote Lorentz indices in n dimensional space. Although W_{ij} is defined in 4 dimensional space, we can still calculate it in n dimensional space first and then project the result to 4 dimensional space, i.e., $W_{ij} = g_{i\mu} g_{j\nu} W^{\mu\nu}$. On the other hand, in the scheme with anti-commuting γ_5, i.e. $\{\gamma_5, \gamma^\mu\} = 0$, the same tensor $W_{\mu\nu}$ can be obtained after one γ_5 in spin projection operators is exchanged with other gamma matrices and then is eliminated by another γ_5 due to $\gamma_5 \gamma_5 = 1$. This is our proof for the equivalence of the two γ_5 schemes for calculations involving transversity PDF. The proof may also help to understand the results of [14,15], where pion and prompt photon as probes of transversity on hadron colliders are explicitly calculated in the two mentioned γ_5 schemes and the same cross sections are obtained. Actually, to all orders of α_s, the two schemes produce the same result. Of course, for scatterings involving other polarized PDFs, like helicity PDF, for which the spin projection operator is $\gamma_5 \gamma^\pm$, we cannot eliminate γ_5 as done in Eq. (49), and we expect the corresponding results in HVBM scheme and anti-commuting scheme are different. Generally, even though there are two γ_5 in a Dirac trace, we still have no reason to claim that HVBM and anti-commuting schemes will generate the same result. For example, $\gamma^\mu \gamma_5 \gamma_\mu \gamma_5 = -4 - \epsilon, -4 + \epsilon$ in HVBM scheme and in anti-commuting scheme, respectively.

4 Numerical results

In this section, we will present our numerical results for A_{TT} defined in Eq. (14), with azimuthal angle integrated over. We consider the heavy quark production on both proton–proton collider and proton–antiproton collider. We know that beyond tree level, the production cross section
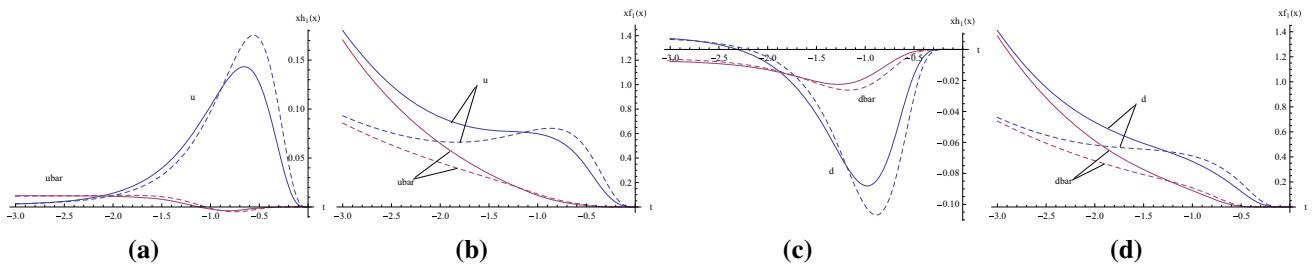
Fig. 5 Transversity PDFs and unpolarized PDFs for u($\bar{u}$) and d($\bar{d}$) quarks at two different scales in our model. In each diagram, the dashed and real lines stand for PDFs at $\mu = 5\,\mathrm{GeV}$ and 60 GeV, respectively. **a** and **c** are for transversity PDFs, while **b** and **d** are for unpolarized PDFs. $x = 10^t$ in each diagram
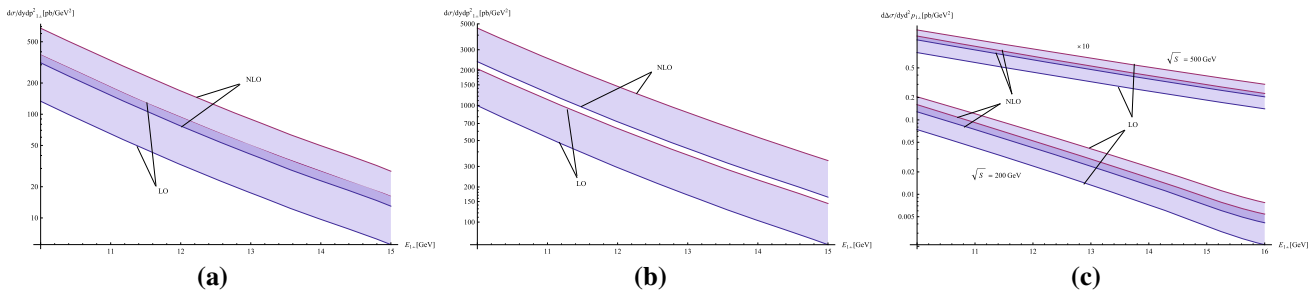
Fig. 6 Unpolarized and polarized cross sections for bottom production on RHIC. **a** and **b** are the unpolarized cross sections for $\sqrt{S} = 200$ and 500 GeV, respectively. **c** is the polarized cross section. In all of these cross sections, we have set rapidity and azimuthal angle of heavy quark to be zero, i.e., $y = 0, \phi = 0$. The uncertainty band is obtained by varying renormalization scale μ from $E_{1\perp}/2$ to $2E_{1\perp}$. Note that in **a**, LO and NLO bands have an overlap

for heavy quark is different from that for heavy anti-quark. Thus, in the following we will also discuss charge average $d\sigma_{ave}$ and charge asymmetry $d\sigma_{asy}$ for both unpolarized and polarized cross sections, which are defined as

$$d\sigma_{ave} \equiv \frac{d\sigma^Q + d\sigma^{\bar{Q}}}{2},$$

$$d\sigma_{asy} \equiv \frac{d\sigma^Q - d\sigma^{\bar{Q}}}{2}. \tag{51}$$

Correspondingly, we define two azimuthal asymmetries A_{TT}^{ave} and A_{TT}^{asy} according to these two different cross sections, respectively. By default, A_{TT} in the following is A_{TT}^{ave}. In the following, leading order (LO) result is tree level result, and next-to-leading order (NLO) result includes tree and one-loop results. Polarizations of (anti-)proton beams are assumed to be one, i.e., $|s_{a\perp}| = |s_{b\perp}| = 1$.

To calculate the cross sections, we need unpolarized PDFs and transversity PDFs. In this work, the unpolarized PDFs are taken as MSTW2008 PDFs [33]. For transversity PDFs, the extracted valence quark transversity PDFs from either TMD formalism or Di-hadron formalism are in agreement with each other within uncertainty range. Thus, we take the extracted transversity PDFs for u, d quarks in [6] as refer-

ence. The remaining sea quark transversity PDFs for $\bar{u}, \bar{d}, \bar{s}$ are still absent in literature, and are assumed to be the same as corresponding sea quark helicity PDFs at a certain low energy scale [9,12,13]. In our case, the low energy scale is $\mu^2 = 2.4\,\mathrm{GeV}^2$, which is the starting scale of [6] for the extraction of transversity PDFs. The helicity PDFs are taken as DSSV type [34,35]. Because unpolarized PDFs are always greater than helicity PDFs for most momentum fraction x, Soffer's bound [36] is always satisfied. Moreover, for unpolarized cross section we use NLO PDFs and NLO α_s, but for polarized cross section we just use LO transversity PDFs and LO α_s. Compared with the evolution of unpolarized PDFs, the scale dependence of transversity PDFs is very small, as shown in Fig. 5. From Fig. 6, the scale uncertainty of polarized cross section by varying renormalization scale μ from $E_{1\perp}/2$ to $2E_{1\perp}$ is much smaller than the scale uncertainty of unpolarized cross section. Thus, we think it is sufficient to use LO transversity PDFs to estimate polarized cross sections.

For bottom production on proton–proton colliders, such as RHIC [16] with $\sqrt{S} = 200, 500\,\mathrm{GeV}$, the cross sections are given in Fig. 6. The hard coefficients of unpolarized cross section are taken from [19]. From LO to NLO, the corrections to unpolarized cross sections are large, which can be greater than 100%, and the scale uncertainty by vary-
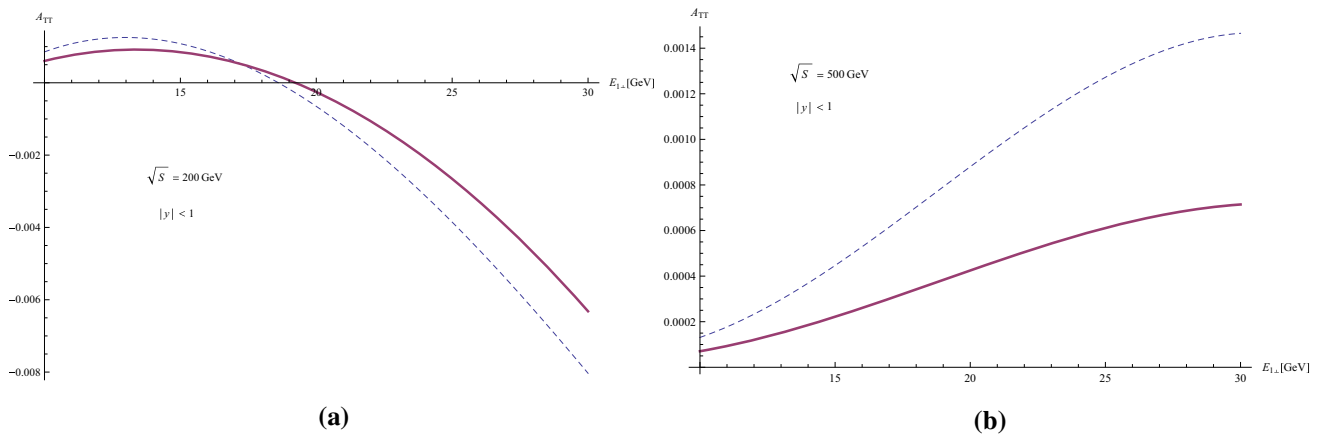
Fig. 7 Azimuthal asymmetries of heavy quark (bottom), in which heavy quark rapidity is integrated over $(-1, 1)$. The dashed line is LO result and the real line is NLO result. The curves are obtained by setting $\mu = E_{1\perp}$

ing renormalization scale μ is not reduced significantly. On the contrary, the scale uncertainty of polarized cross sections is reduced greatly from LO to NLO, as shown in Fig. 6c. Note that the central values of LO and NLO polarized cross sections are very close to each other in this figure, which means the loop correction to polarized cross section is not large. Thus, we conclude the main correction to A_{TT} and the main scale uncertainty are caused by unpolarized cross section. For more precise estimate, one has to use NNLO unpolarized cross section in the denominator of A_{TT}.

As expected, on RHIC due to the smallness of sea transversities, the azimuthal asymmetry A_{TT} is very small. When $E_{1\perp} \leq 15\,\text{GeV}$, A_{TT} is of order 10^{-4}. One can see this from Fig. 7. According to the estimate of [13], the observable asymmetry on RHIC should at least be larger than 10^{-3}. Thus, the observation of A_{TT} on RHIC is very difficult.

Besides the smallness of sea transversities, the very large contribution of gluon to unpolarized cross section also suppresses A_{TT} (or A_{TT}^{ave} explicitly). However, for heavy quark production, the charge asymmetry does not receive contribution from gluon-gluon scattering due to charge conjugation and Bose symmetries. Thus, one may guess A_{TT}^{asy} will be sizable. But this is not the case. For $E_{1\perp} = 10\,\text{GeV}$, A_{TT}^{asy} is shown in Fig. 8 for both cases with $\sqrt{S} = 200, 500\,\text{GeV}$ and $E_{1perp} = 10\,\text{GeV}$. Only for $\sqrt{S} = 200\,\text{GeV}$, A_{TT}^{asy} can reach 10^{-3} in very central region($|y| \leq 0.2$). We note that for unpolarized cross section, $d\sigma^{asy}$ is nearly 2 orders smaller than $d\sigma^{ave}$ in the considering kinematical region. Interestingly, for polarized cross section, $d\Delta\sigma^{asy}$ is also smaller than $d\Delta\sigma^{ave}$ by about 2 orders. Thus, A_{TT}^{asy} actually is of the same order as A_{TT}^{ave}, and can hardly give us more information about transversity.
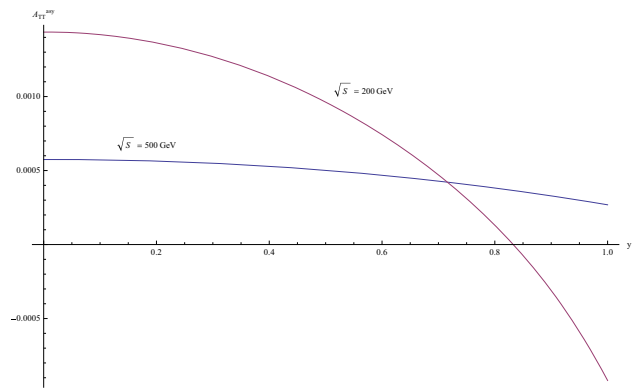
Fig. 8 Azimuthal asymmetry related to heavy quark charge asymmetry, i.e., A_{TT}^{asy}. $E_{1\perp} = 10\,\text{GeV}$ and $\mu = E_{1\perp}$ are taken in the calculation

Since polarized anti-proton beam is not available now, there is no experiment for DSA on proton–antiproton colliders. But an interesting polarized anti-proton program was proposed by PAX collaboration of FAIR at GSI [18]. The main purpose is to measure the lepton angular distribution in double transversely polarized Drell–Yan. There are collider and fixed target schemes. In collider scheme, the momentum of polarized anti-proton can reach $15\,\text{GeV}/c$, and the momentum of polarized proton can reach $3.5\,\text{GeV}/c$. In fixed target scheme, the momentum of polarized anti-proton can reach $22\,\text{GeV}/c$. In collider scheme, charm can be produced. Thus, it is interesting to see whether A_{TT} for charm production can be measured on GSI. Here we consider the charge average only. The resulting A_{TT} is shown in the tables in Appendix C1 in various kinematical regions. From these results, A_{TT} on GSI is above 1%, and in some regions it can be greater than 10%. Thus, measuring A_{TT} for charm production on future GSI experiments will be very helpful to determine or justify the extracted valence transversity PDFs.

5 Summary

In this work, we calculate one-loop QCD correction to single heavy quark inclusive production on double transversely polarized hadron colliders. Analytic results are given. The tensor integrals appearing in both virtual and real corrections are treated similarly and are reduced by FIRE into several master integrals. For real correction, the soft and collinear divergences of master integrals can be separated easily. Then, these master integrals are calculated with Feynman parameters. The results are the same as those in literature [20,21]. As a check, we also use our program to calculate the unpolarized cross section with $q\bar{q}$ as partons entering hard scattering, and numerically, the obtained hard coefficients are the same as known results in literature [19,21]. With the analytic results, numerical estimates on proton–proton collider (RHIC,$\sqrt{S}$ = 200, 500 GeV) and proton–antiproton collider (e.g.,GSI, collider scheme) are given. The azimuthal asymmetry A_{TT} for bottom production on RHIC are suppressed by the smallness of sea transversity PDF and by dominated gluon contribution to unpolarized cross section. The resulting A_{TT} on RHIC is of order 10^{-4}, which is too small to be measured. Even with charge asymmetry of heavy quark production taken into account, the related asymmetry A_{TT}^{asy} is not enhanced greatly. On GSI, valence transversity PDFs give main contribution to A_{TT}. For charm production, A_{TT} can be greater than 10%, which provides a good chance to extract or justify the extracted valence transversity PDFs. Moreover, the main uncertainty of A_{TT} is caused by the large scale dependence of unpolarized cross sections. To get more precise estimates, NNLO unpolarized cross sections should be used.

Data Availability Statement This manuscript has no associated data or the data will not be deposited. [Authors' comment: Up to now, there is no experimental data for the processes we are considering. Thus, we give plots according to our analytic formula with some special parameters to show the effects of one-loop corrections. In the case the experiments are done, one can recalculate the observables using the parameters related to the experiments. As mentioned in the text, one can write to the author by email to obtain the analytical formula, which is too lengthy to be shown in the paper.]

Appendix A: Bubble and tadpole integrals

The bubble and tadpole integrals are defined as

$$
\mu^{4-n} \int \frac{d^n l}{(2\pi)^n} \frac{1}{[l^2 - m_1^2][(l+p)^2 - m_2^2]}
$$

$$
= \frac{i}{16\pi^2} \frac{(4\pi)^{\epsilon/2}}{\Gamma(1 - \epsilon/2)} b(p^2, m_1, m_2),
$$

$$
\mu^{4-n} \int \frac{d^n l}{(2\pi)^n} \frac{1}{l^2 - m^2}
$$

$$
= \frac{i}{16\pi^2} \frac{(4\pi)^{\epsilon/2}}{\Gamma(1 - \epsilon/2)} a_0(m). \tag{A1}
$$

The integrals are expanded to $O(\epsilon)$. The calculation is done in physical region, with $s > 0$, $t < 0$.

1.

$$
b(t, m, 0) = \left(\frac{\mu^2}{m^2}\right)^{\epsilon/2} \left(\frac{m^2 - t}{m^2}\right)^{-\epsilon/2} B(1 - \epsilon/2, \epsilon/2) J
$$

$$
J = 1 - \frac{\epsilon}{2} \left[\frac{m^2 \log\left(\frac{m^2}{m^2 - t}\right)}{t} - 2 \right]
$$

$$
+ \frac{\epsilon^2}{8} \frac{1}{3t} \left[-6 \left(m^2 - t\right) \text{Li}_2 \left(\frac{m^2}{m^2 - t}\right) \right.
$$

$$
+ 3m^2 \log^2\left(\frac{m^2}{m^2 - t}\right) - 6\log\left(\frac{m^2}{m^2 - t}\right)
$$

$$
\times \left(\left(m^2 - t\right)\log\left(\frac{t}{t - m^2}\right) + 2m^2\right)
$$

$$
\left. + \pi^2 m^2 - \pi^2 t + 24t \right], \tag{A2}
$$

2.

$$
b(s, 0, 0) = \left(\frac{\mu^2}{m^2}\right)^{\epsilon/2} B\left(1 - \frac{\epsilon}{2}, \frac{\epsilon}{2}\right) B\left(1 - \frac{\epsilon}{2}, 1 - \frac{\epsilon}{2}\right)
$$

$$
\times \left[1 - \frac{\epsilon}{2} \ln\frac{s}{m^2} + \frac{\epsilon^2}{8} \left(\ln^2\frac{s}{m^2} - \pi^2\right) \right], \tag{A3}
$$

3.

$$b(s, m, m) = \left(\frac{\mu^2}{m^2}\right)^{\epsilon/2} B\left(1 - \frac{\epsilon}{2}, \frac{\epsilon}{2}\right)$$

$$\times \left[1 - \frac{\epsilon}{2}\int_0^1 dx \ln|1 + Ax(1-x)|\right.$$

$$+ \frac{\epsilon^2}{8}\left(-\pi^2\sqrt{1 + 4/A}\right.$$

$$\left.\left. + \int_0^1 dx \ln^2|1 + Ax(1-x)|\right)\right],$$

$$A = \frac{-s}{m^2}, \tag{A4}$$

4.

$$a_0(m) = -\Gamma\left(1 - \frac{\epsilon}{2}\right)\Gamma\left(-1 + \frac{\epsilon}{2}\right)(m^2)^{1-\frac{\epsilon}{2}}$$

$$= \left(\frac{\mu^2}{m^2}\right)^{\epsilon/2}\frac{m^2}{1 - \epsilon/2}B(1 - \epsilon/2, \epsilon/2)$$

$$= \left(\frac{\mu^2}{m^2}\right)^{\epsilon/2}m^2\left[\frac{2}{\epsilon} + 1 + \frac{1}{12}\left(6 + \pi^2\right)\epsilon\right]. \tag{A5}$$

Appendix B: Real integrals

The real integrals defined in Eq. (31) are given here. R_3 is calculated to $O(1)$, and R_6 is calculated to $O(\epsilon^2)$. Others are calculated to $O(\epsilon)$. All are compared with the formulas in [20]. Numerically, the two results are precisely the same. R_i are organized as follows:

$$R_i = N_\epsilon\left[\frac{2}{\epsilon}R_i^{(-1)} + R_i^{(0)} + \frac{\epsilon}{2}R_i^{(1)}\right],$$

$$N_\epsilon = \frac{2\pi^{1-\frac{\epsilon}{2}}}{\Gamma\left(1 - \frac{\epsilon}{2}\right)}. \tag{B.1}$$

The explicit expressions are

$R_1(w)$:

$$R_1^{(-1)} = -4w^2;$$
$$R_1^{(0)} = -8w^2\log(w);$$
$$R_1^{(1)} = 2w^2\left[4\text{Li}_2(1 - 2w) - 2\text{Li}_2(-2w)\right.$$

$$\left. - 2\text{Li}_2\left(\frac{1}{2w + 1}\right) - \log^2(2w + 1)\right.$$

$$+ 2\log(w)\log\left(\frac{32}{2w + 1}\right) - 2\log(2)\log(w(2w + 1))$$

$$\left. + \frac{\pi^2}{3} + 4\log^2(2)\right]; \tag{B.2}$$

$R_2(\delta, w)$:

$$R_2^{(-1)} = -\frac{2w^2}{2w^2(\delta - 1) + 1};$$

$$R_2^{(0)} = \frac{2w^2\log\left(\frac{(2w^2(\delta-1)+1)^2}{w^4(\delta^2-1)}\right)}{2w^2(\delta - 1) + 1};$$

$$R_2^{(1)} = -\frac{w^2}{3\left(2w^2(\delta - 1) + 1\right)}$$

$$\times \left[6\text{Ir2}(\delta, w) - 6\text{Li}_2\left(\frac{w(\delta - 1) + 1}{2(\delta - 1)w^2 + 1}\right)\right.$$

$$+ 3\log\left(\frac{w(2w + 1)}{2w^2(\delta - 1) + 1}\right)$$

$$\times \left(3\log\left(\frac{w}{2w^2(\delta - 1) + 1}\right)\right.$$

$$\left. + 2\log((2w - 1)(\delta - 1)) + \log\left(\frac{1}{4}(2w + 1)\right)\right)$$

$$- 6\log(2)\log\left(\frac{w(2w - 1)(\delta - 1)}{2w^2(\delta - 1) + 1}\right)$$

$$- 3\log\left(\frac{2w^2(\delta + 1)}{4w^2 - 1}\right)$$

$$\times \left(\log\left(16(w(-\delta) + w + 1)^2\right)\right.$$

$$\left. - 2\log(w(\delta - 1) + 1)\right) + \pi^2 + 3\log^2(2)\right];$$

$$\text{Ir2}(\delta, w) = \int_0^1 dz\frac{\xi_3 - \xi_2}{(z + \xi_3)(z + \xi_2)}$$

$$\times \ln\frac{(1 - z)(z + \xi_1)}{(z + \xi_2)|z + \xi_3|} - \int_0^1 dz\frac{1 + \xi_1}{z(1 + \xi_1 - z)}$$

$$\times \ln\frac{(1 - \frac{z}{1+\xi_2})(1 - \frac{z}{1+\xi_3})}{1 - \frac{z}{1+\xi_1}};$$

$$\xi_1 = \frac{w(2w - 1)(\Delta - 1)}{1 + w(\Delta - 1)},$$

$$\xi_2 = 2w - 1, \quad \xi_3 = \frac{w(1 + \Delta)}{1 + w - w\Delta}. \tag{B.3}$$

$R_3(\delta, \Delta, w)$:

$$R_3^{(-1)} = 0;$$

$$R_3^{(0)} = \frac{2w^2}{\sqrt{4w^2\left(w^2(\delta-\Delta)^2+\delta\Delta-1\right)+1}}$$

$$\times \log\left(-\frac{2w^2(\delta\Delta-1)+\sqrt{4w^2\left(w^2(\delta-\Delta)^2+\delta\Delta-1\right)+1}+1}{w^2(2-2\delta\Delta)+\sqrt{4w^2\left(w^2(\delta-\Delta)^2+\delta\Delta-1\right)+1}-1}\right);$$

$$(\text{B.4})$$

R_4:

$$R_4^{(-1)} = -1;$$

$$R_4^{(0)} = 2\log(2);$$

$$R_4^{(1)} = 2\left(\frac{\pi^2}{12} - \log^2(2)\right);$$

$$(\text{B.5})$$

$R_5(\delta)$:

$$R_5^{(-1)} = 0;$$

$$R_5^{(0)} = \log\left(\frac{\delta+1}{\delta-1}\right);$$

$$R_5^{(1)} = -\text{Li}_2\left(-\frac{2}{\delta-1}\right)$$

$$+ \text{Li}_2\left(\frac{2}{\delta+1}\right) - 2\log(2)\log\left(\frac{\delta+1}{\delta-1}\right);$$

$$(\text{B.6})$$

R_6:

$$R_6 = \int d\Omega_{n-1} = N_\epsilon \int_0^\pi d\theta \sin^{n-3}\theta$$

$$= N_\epsilon 2^{1-\epsilon} B\left(1-\frac{\epsilon}{2}, 1-\frac{\epsilon}{2}\right)$$

$$= N_\epsilon\left[2 + \epsilon(2-\log(4)) + \epsilon^2\left(2 - \frac{\pi^2}{12}\right.\right.$$

$$\left.\left. + \log^2(2) - \log(4)\right) + O(\epsilon^3)\right].$$

$$(\text{B.7})$$

Appendix C: Numerical results on GSI

Numerical results for charm production on GSI are listed in following tables. In the unpolarized cross sections the azimuthal angle of heavy quark is integrated over, and we show the results for

$$\frac{d\sigma^{unp}}{dy d\vec{p}_{1\perp}^2} = \pi \frac{d\sigma^{unp}}{dy d^2 p_{1\perp}}, \tag{C.1}$$

where the differential cross section on right-hand side is defined in Eq. (9). Further, the contributions from different parton flavors in initial state of subprocess are also shown in the following tables. That is,

$$\frac{d\sigma^{unp}}{dy d\vec{p}_{1\perp}^2} = \sum_{(ij)=gg,qg,q\bar{q}} \frac{d\sigma_{ij}^{unp}}{dy d\vec{p}_{1\perp}^2}. \tag{C.2}$$

$d\sigma_{gg}$ is the cross section given by subprocess $gg \to Q+X$; $d\sigma_{qg}$ is the cross section given by subprocesses $qg \to Q+X$ and $gq \to Q+X$, with $q = u, d, s, \bar{u}, \bar{d}, \bar{s}$; $d\sigma_{q\bar{q}}$ is the cross section given by subprocesses $q\bar{q} \to Q+X$, with $q\bar{q} = u\bar{u}, d\bar{d}, s\bar{s}, \bar{u}u, \bar{d}d, \bar{s}s$. For convenience, following notations are introduced:

$$\Sigma_{ij} \equiv \frac{d\sigma_{ij}^{unp}}{dy d\vec{p}_{1\perp}^2},$$

$$\Sigma \equiv \sum_{ij} \Sigma_{ij} = \frac{d\sigma^{unp}}{dy d\vec{p}_{1\perp}^2},$$

$$\Sigma_T \equiv \frac{d\Delta\sigma}{dy d^2 p_{1\perp}}\bigg|_{\phi=0,|s_{a\perp}|=|s_{b\perp}|=1}. \tag{C.3}$$

For polarized cross section, it is clear that $d\Delta\sigma = d\Delta\sigma_{q\bar{q}}$, and quark flavors $q\bar{q}$ are the same as those of unpolarized cross section. In polarized cross section we have set the azimuthal angle of heavy quark to be zero, and assumed the polarizations of initial (anti-)proton beams to be 1. With these notations, the azimuthal asymmetry $A_{TT} = \frac{\pi}{2}\frac{\Sigma_T}{\Sigma}$.

Moreover, as illustrated in text, all cross sections here are for the charge average of heavy quark, i.e. $d\sigma_{ave}$ defined in Eq. (51). The renormalization scale dependence(μ dependence) is also calculated. As done in [19], each cross section is calculated by setting $\mu = \mu_0/2, \mu_0, 2\mu_0$ with $\mu_0 = E_{1\perp}$. In following tables, corresponding to every $(E_{1\perp}, y)$, the central number is given by $\mu = \mu_0$, while the upper and lower numbers are given by $\mu = \mu_0/2, 2\mu_0$, respectively. For the case $E_{1\perp} = 3\,\text{GeV}$, $\mu_0/2$ is replaced by $\sqrt{2.4}\,\text{GeV}$. The unit of $E_{1\perp}$ is GeV and the unit of cross section is pb/GeV^2. Charm mass $m_c = 1.40\,\text{GeV}$ and bottom mass $m_b = 4.75\,\text{GeV}$. All calculations are performed in $\overline{\text{MS}}$ scheme.

1. Results on GSI $S = 216.4\,\text{GeV}^2$

GSI $S = 216.4\text{GeV}^2$ $E_{1\perp} = 3\text{GeV}$	$\Sigma_{gg}(pb/\text{GeV}^2)$	$\Sigma_{qg}(pb/\text{GeV}^2)$	$\Sigma_{q\bar{q}}(pb/\text{GeV}^2)$	$\Sigma(pb/\text{GeV}^2)$	$\Sigma_T(pb/\text{GeV}^2)$	A_{TT}
$y = 0.0$	2.59×10^3	2.60×10^2	8.52×10^3	1.14×10^4	1.58×10^2	2.18×10^{-2}
	8.64×10^2	-2.22×10	5.73×10^3	6.58×10^3	1.79×10^2	4.26×10^{-2}
	3.02×10^2	-2.26×10	3.22×10^3	3.50×10^3	1.17×10^2	5.24×10^{-2}
$y = 0.3$	2.36×10^3	2.09×10^2	7.15×10^3	9.72×10^3	1.33×10^2	2.16×10^{-2}
	7.53×10^2	-2.09×10	4.80×10^3	5.53×10^3	1.48×10^2	4.20×10^{-2}
	2.57×10^2	-1.93×10	2.67×10^3	2.91×10^3	9.55×10	5.15×10^{-2}
$y = 0.6$	1.66×10^3	1.01×10^2	4.02×10^3	5.78×10^3	7.66×10	2.08×10^{-2}
	4.67×10^2	-1.50×10	2.66×10^3	3.11×10^3	7.90×10	3.99×10^{-2}
	1.47×10^2	-1.09×10	1.44×10^3	1.58×10^3	4.92×10	4.89×10^{-2}
$y = 0.9$	7.18×10^2	2.03×10	1.22×10^3	1.96×10^3	2.40×10	1.93×10^{-2}
	1.59×10^2	-5.66	7.76×10^2	9.30×10^2	2.15×10	3.64×10^{-2}
	4.27×10	-3.02	4.01×10^2	4.41×10^2	1.24×10	4.43×10^{-2}
$y = 1.2$	9.02×10	3.49×10^{-2}	9.70×10	1.87×10^2	1.91	1.60×10^{-2}
	1.27×10	-4.39×10^{-1}	5.46×10	6.69×10	1.29	3.03×10^{-2}
	2.49	-1.51×10^{-1}	2.51×10	2.74×10	6.38×10^{-1}	3.66×10^{-2}
GSI $S = 216.4\text{GeV}^2$ $E_{1\perp} = 4\text{GeV}$	$\Sigma_{gg}(pb/\text{GeV}^2)$	$\Sigma_{qg}(pb/\text{GeV}^2)$	$\Sigma_{q\bar{q}}(pb/\text{GeV}^2)$	$\Sigma(pb/\text{GeV}^2)$	$\Sigma_T(pb/\text{GeV}^2)$	A_{TT}
$y = 0.0$	3.46×10	2.46	2.53×10^2	2.90×10^2	1.37×10	7.38×10^{-2}
	9.90	-2.55×10^{-1}	1.77×10^2	1.87×10^2	1.22×10	1.03×10^{-1}
	3.10	-2.10×10^{-1}	9.98×10	1.03×10^2	9.42	1.44×10^{-1}
$y = 0.3$	2.82×10	1.56	1.84×10^2	2.14×10^2	9.79	7.20×10^{-2}
	7.48	-2.15×10^{-1}	1.28×10^2	1.35×10^2	8.53	9.94×10^{-2}
	2.25	-1.54×10^{-1}	7.11×10	7.32×10	6.53	1.40×10^{-1}
$y = 0.6$	1.25×10	2.79×10^{-1}	5.97×10	7.24×10	3.06	6.63×10^{-2}
	2.62	-9.05×10^{-2}	4.01×10	4.26×10	2.42	8.94×10^{-2}
	6.87×10^{-1}	-4.69×10^{-2}	2.14×10	2.20×10	1.80	1.29×10^{-1}
$y = 0.9$	1.14	-7.02×10^{-3}	3.71	4.85	1.69×10^{-1}	5.48×10^{-2}
	1.47×10^{-1}	-5.24×10^{-3}	2.15	2.29	1.04×10^{-1}	7.11×10^{-2}
	2.87×10^{-2}	-1.74×10^{-3}	1.02	1.05	7.18×10^{-2}	1.08×10^{-1}
GSI $S = 216.4\text{GeV}^2$ $E_{1\perp} = 5\text{GeV}$	$\Sigma_{gg}(pb/\text{GeV}^2)$	$\Sigma_{qg}(pb/\text{GeV}^2)$	$\Sigma_{q\bar{q}}(pb/\text{GeV}^2)$	$\Sigma(pb/\text{GeV}^2)$	$\Sigma_T(pb/\text{GeV}^2)$	A_{TT}
$y = 0.0$	3.33×10^{-1}	4.43×10^{-3}	5.21	5.55	5.03×10^{-1}	1.43×10^{-1}
	7.56×10^{-2}	-2.86×10^{-3}	3.47	3.55	3.73×10^{-1}	1.65×10^{-1}
	1.97×10^{-2}	-1.38×10^{-3}	1.87	1.89	2.06×10^{-1}	1.72×10^{-1}
$y = 0.3$	2.06×10^{-1}	4.62×10^{-4}	2.86	3.07	2.61×10^{-1}	1.34×10^{-1}
	4.13×10^{-2}	-1.64×10^{-3}	1.84	1.88	1.85×10^{-1}	1.55×10^{-1}
	1.00×10^{-2}	-7.00×10^{-4}	9.62×10^{-1}	9.71×10^{-1}	9.89×10^{-2}	1.60×10^{-1}
$y = 0.6$	2.33×10^{-2}	-3.38×10^{-4}	2.53×10^{-1}	2.76×10^{-1}	1.88×10^{-2}	1.07×10^{-1}
	3.08×10^{-3}	-1.19×10^{-4}	1.37×10^{-1}	1.40×10^{-1}	1.09×10^{-2}	1.22×10^{-1}
	5.94×10^{-4}	-3.73×10^{-5}	6.45×10^{-2}	6.50×10^{-2}	5.20×10^{-3}	1.26×10^{-1}
GSI $S = 216.4\text{GeV}^2$ $E_{1\perp} = 6\text{GeV}$	$\Sigma_{gg}(pb/\text{GeV}^2)$	$\Sigma_{qg}(pb/\text{GeV}^2)$	$\Sigma_{q\bar{q}}(pb/\text{GeV}^2)$	$\Sigma(pb/\text{GeV}^2)$	$\Sigma_T(pb/\text{GeV}^2)$	A_{TT}
$y = 0.0$	8.39×10^{-4}	-1.94×10^{-5}	3.20×10^{-2}	3.28×10^{-2}	3.90×10^{-3}	1.87×10^{-1}
	1.24×10^{-4}	-5.61×10^{-6}	1.66×10^{-2}	1.68×10^{-2}	2.15×10^{-3}	2.02×10^{-1}
	2.42×10^{-5}	-1.69×10^{-6}	7.73×10^{-3}	7.76×10^{-3}	1.01×10^{-3}	2.04×10^{-1}
$y = 0.3$	2.06×10^{-4}	-4.77×10^{-6}	7.32×10^{-3}	7.52×10^{-3}	7.96×10^{-4}	1.66×10^{-1}
	2.54×10^{-5}	-1.06×10^{-6}	3.44×10^{-3}	3.46×10^{-3}	3.92×10^{-4}	1.78×10^{-1}
	4.92×10^{-6}	-2.95×10^{-7}	1.50×10^{-3}	1.51×10^{-3}	1.72×10^{-4}	1.79×10^{-1}

Appendix D: Notes for mathematica programs

- `hdTree`: $h_d^{(0)}(\tau_1, \rho)$;
- `hdLoop`: $h_d^{(1)}(\tau_1, \rho)$;
- `hpLarge`: $h_p^{(1)}(\tau_x, \tau_1, \rho)$;
- `hpSmall`: $h_p^{(1)}$ with τ_x expanded to $O(\tau_x^4)$;
- `hL`: $h_l^{(1)}(\tau_x, \tau_1, \rho)$.

Some parameters are introduced to give results in different schemes. In $\overline{\text{MS}}$-scheme,

$$\text{tep} = 1, \ \text{tct} = 0, \ \text{nc} = \text{nb} = 1, \ \text{nF} = 3. \tag{D1}$$

In zero-momentum subtraction of [19], for bottom production,

$$\text{tep} = 1, \ \text{tct} = 1, \ \text{nc} = 0, \ \text{nb} = 1, \ \text{nF} = 4. \tag{D2}$$

and for charm production,

$$\text{tep} = 1, \ \text{tct} = 1, \ \text{nc} = 1,$$
$$\text{nb} = 0, \ \text{nF} = 3. \tag{D3}$$

Other parameters are common, which are color factors and kinematical variables:

$$N_1 = N_c C_F^2, \ N_2 = C_A N_c C_F^2, \ N_3 = N_c C_F, \ ncolor = N_c,$$
$$\rho_b = \frac{4m_b^2}{s}, \ \rho_c = \frac{4m_c^2}{s}, \ L_\mu = \ln \frac{\mu^2}{m^2}. \tag{D4}$$

An example is given for unpolarized hard coefficients.

References

1. J.P. Ralston, D.E. Soper, Nucl. Phys. B **152**, 109 (1979). https://doi.org/10.1016/0550-3213(79)90082-8
2. R.L. Jaffe, X.-D. Ji, Phys. Rev. Lett. **67**, 552 (1991). https://doi.org/10.1103/PhysRevLett.67.552
3. R.L. Jaffe, X.-D. Ji, Nucl. Phys. B **375**, 527 (1992). https://doi.org/10.1016/0550-3213(92)90110-W
4. J.L. Cortes, B. Pire, J.P. Ralston, Z. Phys. C **55**, 409 (1992). https://doi.org/10.1007/BF01565099
5. M. Anselmino, M. Boglione, U. D'Alesio, S. Melis, F. Murgia, A. Prokudin, Phys. Rev. D **87**, 094019 (2013). https://doi.org/10.1103/PhysRevD.87.094019. arXiv:1303.3822 [hep-ph]
6. Z.-B. Kang, A. Prokudin, P. Sun, F. Yuan, Phys. Rev. D **93**, 014009 (2016). https://doi.org/10.1103/PhysRevD.93.014009. arXiv:1505.05589 [hep-ph]
7. H.-W. Lin, W. Melnitchouk, A. Prokudin, N. Sato, H. Shows, Phys. Rev. Lett. **120**, 152502 (2018). https://doi.org/10.1103/PhysRevLett.120.152502. arXiv:1710.09858 [hep-ph]
8. M. Radici, A. Bacchetta, Phys. Rev. Lett. **120**, 192001 (2018). https://doi.org/10.1103/PhysRevLett.120.192001. arXiv:1802.05212 [hep-ph]
9. V. Barone, A. Cafarella, C. Coriano, M. Guzzi, P. Ratcliffe, Phys. Lett. B **639**, 483 (2006). https://doi.org/10.1016/j.physletb.2006.07.012. arXiv:hep-ph/0512121 [hep-ph]
10. H. Shimizu, G.F. Sterman, W. Vogelsang, H. Yokoya, Phys. Rev. D **71**, 114007 (2005). https://doi.org/10.1103/PhysRevD.71.114007. arXiv:hep-ph/0503270 [hep-ph]
11. H. Kawamura, J. Kodaira, K. Tanaka, Nucl. Phys. B **777**, 203 (2007). https://doi.org/10.1016/j.nuclphysb.2007.04.022. arXiv:hep-ph/0703079 [hep-ph]
12. D. de Florian, Phys. Rev. D **96**, 094006 (2017). https://doi.org/10.1103/PhysRevD.96.094006. arXiv:1711.01235 [hep-ph]
13. J. Soffer, M. Stratmann, W. Vogelsang, Phys. Rev. D **65**, 114024 (2002). https://doi.org/10.1103/PhysRevD.65.114024. arXiv:hep-ph/0204058 [hep-ph]
14. A. Mukherjee, M. Stratmann, W. Vogelsang, Phys. Rev. D **67**, 114006 (2003). https://doi.org/10.1103/PhysRevD.67.114006. arXiv:hep-ph/0303226 [hep-ph]
15. A. Mukherjee, M. Stratmann, W. Vogelsang, Phys. Rev. D **72**, 034011 (2005). https://doi.org/10.1103/PhysRevD.72.034011. arXiv:hep-ph/0506315 [hep-ph]
16. E.C. Aschenauer et al. (2013) arXiv:1304.0079 [nucl-ex]
17. V. Barone et al. (PAX) (2005). arXiv:hep-ex/0505054 [hep-ex]
18. P. Lenisa et al., *Proceedings, 2nd High-Energy Physics Conference in Madagascar (HEP-MAD 04): Antananarivo, Madagascar, September 27-October 3, 2004*, eConf **C0409272**, 014 (2004). arXiv:hep-ex/0412063 [hep-ex]
19. P. Nason, S. Dawson, R.K. Ellis, Nucl. Phys. B **327**, 49 (1989) [Erratum: Nucl. Phys. B **335**, 260 (1990)]. https://doi.org/10.1016/0550-3213(89)90286-1
20. W. Beenakker, H. Kuijf, W.L. van Neerven, J. Smith, Phys. Rev. D **40**, 54 (1989). https://doi.org/10.1103/PhysRevD.40.54
21. W. Beenakker, W.L. van Neerven, R. Meng, G.A. Schuler, J. Smith, Nucl. Phys. B **351**, 507 (1991). https://doi.org/10.1016/S0550-3213(05)80032-X
22. S. Catani, S. Devoto, M. Grazzini, S. Kallweit, J. Mazzitelli, JHEP **07**, 100 (2019). https://doi.org/10.1007/JHEP07(2019)100. arXiv:1906.06535 [hep-ph]
23. J. Collins, Camb. Monogr. Part. Phys. Nucl. Phys. Cosmol. **32**, 1 (2011)
24. A.V. Smirnov, JHEP **10**, 107 (2008). https://doi.org/10.1088/1126-6708/2008/10/107. arXiv:0807.3243 [hep-ph]
25. R.K. Ellis, G. Zanderighi, JHEP **02**, 002 (2008). https://doi.org/10.1088/1126-6708/2008/02/002. arXiv:0712.1851 [hep-ph]
26. C. Anastasiou, K. Melnikov, Nucl. Phys. B **646**, 220 (2002). https://doi.org/10.1016/S0550-3213(02)00837-4. arXiv:hep-ph/0207004 [hep-ph]
27. J.C. Collins, T.C. Rogers, Phys. Rev. D **78**, 054012 (2008). https://doi.org/10.1103/PhysRevD.78.054012. arXiv:0805.1752 [hep-ph]
28. R. Brock et al., (CTEQ). Rev. Mod. Phys. **67**, 157 (1995). https://doi.org/10.1103/RevModPhys.67.157
29. A. Mukherjee, D. Chakrabarti, Phys. Lett. B **506**, 283 (2001). https://doi.org/10.1016/S0370-2693(01), 00364–1. arXiv:hep-ph/0102003 [hep-ph]
30. J. Blumlein, Eur. Phys. J. C **20**, 683 (2001). https://doi.org/10.1007/s100520100703. arXiv:hep-ph/0104099 [hep-ph]
31. G. 't Hooft , M.J.G. Veltman, Nucl. Phys. B **44**, 189 (1972). https://doi.org/10.1016/0550-3213(72)90279-9
32. P. Breitenlohner, D. Maison, Commun. Math. Phys. **52**, 11 (1977). https://doi.org/10.1007/BF01609069

33. A.D. Martin, W.J. Stirling, R.S. Thorne, G. Watt, Eur. Phys. J. C **63**, 189 (2009). https://doi.org/10.1140/epjc/s10052-009-1072-5. arXiv:0901.0002 [hep-ph]

34. D. de Florian, R. Sassot, M. Stratmann, W. Vogelsang, Phys. Rev. D **80**, 034030 (2009). https://doi.org/10.1103/PhysRevD.80.034030. arXiv:0904.3821 [hep-ph]

35. D. de Florian, R. Sassot, M. Stratmann, W. Vogelsang, Phys. Rev. Lett. **113**, 012001 (2014). https://doi.org/10.1103/PhysRevLett.113.012001. arXiv:1404.4293 [hep-ph]

36. J. Soffer, Phys. Rev. Lett. **74**, 1292 (1995). https://doi.org/10.1103/PhysRevLett.74.1292. arXiv:hep-ph/9409254 [hep-ph]